International Journal of Nanomedicine

Dovepress
open access to scientific and medical research

Open Access Full Text Article

ORIGINAL RESEARCH

Antibiotic-Loaded MMT/PLL-Based Coating on the Surface of Endosseous Implants to Suppress Bacterial Infections

Xingfang Yu[1,*]
Xin Liao[2,*]
Hongwei Chen[1]

[1]Department of Orthopedics, The Affiliated Yiwu Hospital of Wenzhou Medical University, Yiwu, Zhejiang, 322000, People's Republic of China; [2]Department of Orthopedics, The Second Affiliated Hospital and Yuying Children's Hospital of Wenzhou Medical University, Wenzhou, Zhejiang, 325000, People's Republic of China

*These authors contributed equally to this work

Background: Bone infections remain one of the most common and serious complications of orthopedic surgery, posing a tremendous economic burden to society and patients. This is because bacteria colonize and multiply on the surface of the implant. The $(MMT/PLL)_8$ multilayer films have been shown to effectively release antibiotics depending on the changes in the microenvironment. Here, vancomycin was loaded into the $(MMT/PLL)_8$ multilayer films, which were prepared to be used as a local delivery system for the treatment of bone infections.

Methods: We used the layer-by-layer self-assembly method to prepare VA-loaded coatings $(MMT/PLL\text{-}VA)_8$ consisting of montmorillonite (MMT), poly-L-lysine (PLL), and VA. The thickness and surface morphology of coatings were characterized using spectroscopic ellipsometry and scanning electron microscopy (SEM). In order to evaluate the drug release behavior from coatings in different media, we measured the size of the zone of inhibition. Additionally, in vitro antibacterial activity was assessed using the shake-flask culture method and SEM images, while that of in vivo was evaluated by establishing an animal model of bone infection.

Results: Our findings revealed that small-molecule antibiotics were successfully loaded into the $(MMT/PLL\text{-}VA)_8$ multilayer film structure during the hierarchical self-assembly process and subsequently the multilayer film structure depicted linear growth behavior. The PLL in the multilayer films was progressively degraded which triggered the VA release when contacted with CMS or bacterial infections. The release of VA from multilayer film structure depends on the concentration changes of CMS. Notably, the multilayer films presented great in vitro cell compatibility. Moreover, the prepared antibacterial multilayer films showed excellent antibacterial property by killing more than 99.99% of *S. aureus* in 24 h. More importantly, we found that multilayer film exhibits good sterilization effect and biocompatibility under the stimulation of bacterial liquid both in vitro and in vivo antibacterial ability tests.

Conclusion: Altogether, this study shows that $(MMT/PLL\text{-}VA)_8$ multilayer films containing CMS and bacteria-responsive drug release properties posess high bactericidal activity and good biocompatibility. This finding provides a novel strategy for the treatment of bone infections.

Keywords: bone infections, multilayer films, microenvironment, layer-by-layer, antibacterial

Correspondence: Hongwei Chen
Department of Orthopedics, The Affiliated Yiwu Hospital of Wenzhou Medical University, Yiwu, Zhejiang, 322000, People's Republic of China
Tel +86-13506896988
Email sssaaa18@163.com

Introduction

With recent advances in material science and medical level techniques, the rate of orthopedic surgery accompanied by the use of endosseous implants are growing rapidly. Bone infections are one of the most prevalent and serious complications of elective orthopedic surgery.[1] A recent study showed that once the implant is placed

in the body, especially in open fractures, it will significantly increase the possibility of infection.[2] Bacteria that adhere to the surface of the implant will reproduce and produce microbial biofilms.[3,4] In particular, bacterial biofilms are renowned for their enhanced resistance to environmental and chemical stresses such as antibiotics, metal ions, and organic solvents.[3–5] Bone infections have become one of the most challenging and persistent health problems facing orthopedists.[6] According to the latest global estimates, about 5% of people using endosseous implants have developed infections in the United States. In the UK, it has been projected that around 7.1 billion pounds are spent to treat implant-related infection each year.[7,8] It has been noted that the infections associated with endosseous implants pose a serious economic burden to society and patients. If the infection control effect is not effective, it can also lead to multiple debridements and surgical revisions, amputation, and eventually death.[9–11] Infections related to endosseous implants have long been one of the research focuses. Many laboratory research work has been devoted to directly kill bacteria and resist bacterial adhesion on the surface of the implant.[12,13] Nowadays, there's also growing interest in antibacterial application of controlled release delivery system. For example, Huang et al developed the EGCG/HPMC membrane that release EGCG and H2O2 upon pH-induced structural changes, thereby killing bacteria on demand.[14] Chambre et al made a photothermal device that releases highly effective antibacterial peptide upon NIR exposure.[15] Hu et al reported a facile chemistry to prepare aminoglycoside hydrogels for on-demand drug delivery.[16] Huang et al combined an injectable hydrogel with porous PLGA microspheres to prepare a continuous drug delivery system that sequentially releases vancomycin to kill bacteria.[17] Studies have reported that, following tissue infection, the microenvironment usually changes due to hypoxic metabolism, decrease in pH, and abnormal expression of enzyme.[18–20] Therefore, using the special biological characteristics of bacterial infection microenvironment to prepare an intelligent drug delivery system with microenvironment response to achieve controlled release and high concentration aggregation of antibacterial drugs at the site of infection is a hotspot of current research.

Layer-by-layer (LbL) self-assembly method, as a novel technology for preparing nano-films, was originally proposed by Decher and Hong in 1991.[21,22] Nowadays, it has become a vital method for constructing multifunctional surfaces due to its easy operation and wide range of applications.[22] The principal driving force for LBL includes electrostatic forces,[23] hydrogen bond, hydrophobic bond, and covalent bond. Likewise, other forces can also form alternating multilayers using similar principles.[24–26] LBL possesses unique benefits, such as easy to process and also physical and chemical properties of this type of multilayers can be easily adjusted by changing the number of layers of the self-assembled multilayers and the type of polyelectrolyte. Collectively, these features substantially expand the application range of layer-by-layer self-assembly multilayers, leading to this multilayer technology become an indispensable method for constructing composite functional films and drug carriers in medical materials.[27] Moreover, the multilayer films can absorb a large amount of free water, thus making the surface of base material much more hydrophilic, which can effectively reduce bacterial adhesion.[28]

Antibiotics are extensively used to prevent or treat implant infections in orthopedics. These compounds constitute important substances used to prepare antibacterial coatings for internal implants.[29] Recently, researchers have made significant progress in designing antibacterial coatings for orthopedic implants through layer-by-layer assembly technology.

For example, researchers used vancomycin-coated titanium alloy steel implants for fixation in the sheep tibial shaft fracture models, while the control group used ordinary titanium alloy steel implants. Then, the two groups of animals were given *S. aureus* at the tibial shaft fracture sites. Animals in the control group formed obvious suppurative osteomyelitis and biofilm, while no infection or biofilm occurred in the animals in the experimental group.[30] Mochalin et al found that through the combined application of a systemic antibiotic treatment, NDs loaded with the antibiotic system can markedly improve the prevention and treatment of implant infections.[31] In another study, Popat et al observed that titanium nanotubes can also be loaded with antibiotics and modified on the surface of implants, which can achieve the release of antibiotics, exerting an essential role in killing microorganisms that adhere to the surface of implants as well as prevent the formation of biofilm.[32] However, excessive antibacterial release from the antibacterial coatings induces bacteria to develop resistance to antibiotics. The major setback is the lack of barriers to prevent drug release.

When bacterial infections occur on the surface of the orthopedic implants, the microenvironment largely changes such as an increase in the concentration of

specific enzyme, pH reduction, and release of complex virulence factor.[33–35] Chymotrypsin (CMS) and hyaluronidase (HAS) concentration largely increase in the infected microenvironment that can be used to trigger antibiotic release from the matrices.[36,37] Recent studies have confirmed that using vancomycin is a vital treatment for orthopedic implant infections, exhibiting strong activity against Gram-positive bacteria.[6,38] At the same time, in vitro experiments have demonstrated that vancomycin exerts fewer negative effects on osteoblasts and skeletal cells compared with other commonly used antibiotics.[39,40] Researchers have developed an antibacterial multilamellar membrane structure by the assembly of montmorillonite (MMT) and poly-L-lysine (PLL). The antibacterial multilayer film structure elucidated effective self-defense property precisely triggered by enzyme change of the microenvironment due to bacteria.[41] In this study, we embedded VA in the $(MMT/PLL\text{-}VA)_8$ multilayer film structure through electrostatic interaction. And CMS also hydrolyzes the C-terminal peptide bonds of PLL to release hydrophobic amino acids.[42] In practice, PLL in the $(MMT/PLL\text{-}VA)_8$ multilayer film structure would be gradually degraded, which then triggers the release of VA when contacted with CMS or bacterial infections.

Materials and Methods

Reagents and Materials

Titanium Kirschner wires (K-wires, 1.25 mm) were purchased from MK Medical GmbH & Co. Poly-L-lysine hydrobromide (PLL, Mw: 4000–15,000 by viscosity), chymotrypsin (CMS, α-chymotrypsin from bovine pancreas, Type II, ≥40 units/mg protein), polyethyleneimine (PEI, Mw: 25 kDa) and VA were bought from Sigma-Aldrich. Ultrapure distilled water was obtained from a Milli-Q purification system (Millipore, Billerica, Massachusetts).

Construction of the $(MMT/PLL\text{-}VA)_8$ Multilayer Films

For this study, glass discs, silicon wafer substrates, and K-wires were cleaned with ethanol and water before use. We prepared MMT stock solution (5 mg/mL) 15 days before use. Subsequently, the MMT stock solution was diluted into 0.5 mg/mL to obtain the MMT deposition solutions, which were dispersed using ultrasonic treatment overnight. Then, PLL and Van in water were dissolved at 1.0 mg/mL and 0.5 mg/mL separately for $(MMT/PLL\text{-}VA)_8$ multilayer film deposition. Substrates were deposited firstly in PEI solution (5 mg/mL) at 37°C for 30 min for a precursor. To construct the $(MMT/PLL\text{-}VA)_8$ multilayer films, we first dipped the substrates in the MMT solution for 15 min and then rinsed 5 times with buffer solution. The films were dried under a gentle stream of nitrogen. We next dipped the substrates in PLL-VA solution for 15 min, followed by rinsing 5 times with buffer solution. This dipping cycle corresponded to the deposition of one bilayer. We consecutively repeated the deposition process until the $(MMT/PLL\text{-}VA)_8$ multilayer films were fabricated through supramolecular complexation.

Characterization of the Multilayer Films

During the preparation of multilayer films, the changes in thickness were followed using spectroscopic ellipsometry (M-2000 DITM, J.A. Woollam). This experiment was performed on silicon wafers. The continuing wavelength ranging from 124 nm to 1700 nm and selected the angle of incidence of both 65ºand 70º for ellipsometry measurements. We selected Δ and Ψ values surveyed at a wavelength of 600–1700 nm for analysis. The thickness of multilayer films was determined using the Cauchy model. We set parameters A_n and B_n for the Cauchy layer at 1.45 and 0.01, respectively, as fit parameters. Then, the thickness that fit the multilayer films was fabricated such that it can be automatically calculated. Further, the morphology of the multilayer films was examined under Hitachi S-4800 electron microscope (Tokyo, Japan) at an acceleration voltage of 10kV. Finally, images were adjusted for clear visualization of the multilayer films and photographed.

Responsive Degradation of the Multilayer Films

For this experiment, the fabricated multilayer films were deposited in 0.01M PBS, CMS (100U/mL) solutions, and *Staphylococcus aureus* (*S. aureus*, ATCC 27217) at the concentration of 10^5 CFU/mL for 6 days. All samples were taken at the same time and dried with nitrogen.

Release of VA from $(MMT/PLL\text{-}VA)_8$ Multilayer Films

In this experiment, zone of bacterial inhibition (ZOI) was used to evaluate the drug release. Specifically, Took 100 μL of Staphylococcus aureus, dropped in the middle of the nutrient agar, evenly coated. Samples were placed on each nutrient agar medium, placed in a 37°C incubator, and cultured for 24 h to observe the results. ZOI was measured with a ruler and recorded, and the average value was calculated.

Cytocompatibility

Bone tissues were collected in accordance with the terms of the Medical Ethical Committee of the Affiliated Yiwu Hospital, Wenzhou Medical University, and following the guidelines of the Declaration of Helsinki. The samples of human bone tissues were obtained from OA patients undergoing total hip arthroplasty (n = 8, range 53–69 years) in the Affiliated Yiwu Hospital of Wenzhou Medical University. Full informed consent was obtained from all patients. Specifically, the osteoblasts were grown in DMEM medium supplemented with 100U/mL penicillin, 10% fetal bovine serum and 100 μg/mL streptomycin in a standard incubator. Confluent cells were digested by 0.25% trypsin-0.02% EDTA, then followed by centrifugation (1000 g for 3 min) in order to harvest the cells. Subsequently, osteoblasts were digested again and resuspended for cultivation on the corresponding materials surface.

In this research, we used the MTT assay to analyze the effect of $(MMT/PLL\text{-}VA)_8$ multilayer films on the proliferation of human osteoblasts. The osteoblasts were planted onto the specimens by the density of 1.0×10^4 cells per sample by using 96-well tissue culture plate, and cell proliferation after 1, 3, 5 and 7 days of culture. Then, phosphate-buffered saline (PBS) was used to rinse the cells and added MTT solution. Removed the MTT solution after incubation in the dark for 4 h. Let the formazan in the cells released through adding DMSO at room temperature. Used a microplate reader to measure absorbance at 570 nm. All experimental measurements were performed with 10 replicates and in 5 independent experiments.

In vitro Antimicrobial Activity

Scanning Electron Microscopy (SEM) Analysis of *S. aureus*

In this subsection, unmodified silicon wafers and $(MMT/PLL\text{-}VA)_8$ multilayer films silicon wafers were prepared. Then, each set of 5 parallel samples was immersed in 1 mL of *S. aureus* suspension (10^2 CFU/mL) and incubated at 37°C. After incubation for 8 h, the surfaces were then thoroughly rinsed with PBS, followed by fixation with 4% cold glutaraldehyde for half an hour. After fixation, the bacteria-adhered surfaces were de-hydrated with an alcohol gradient. Specifically, they were dehydrated in a growing ethanol solution gradients: 50, 60, 70, 80, 90, and 99% (v/v), for 15 min each. Subsequently, the bacteria-adhered surfaces were dried in an oven at 40°C. Prior to examination, these surfaces were gold sputter-coated to make them electrically conductive. Eventually, all samples were characterized using Quanta 450 FEG SEM.

Inhibition Rate Assays

In this experiment, we employed the shake-flask culture method with *S. aureus* to test the antibacterial effect of the multilayer films. We specifically placed the $(MMT/PLL\text{-}VA)_8$ multilayer films coated with PDMS into test tubes, containing 10 mL of 1.5×10^4 CFU/mL of *S. aureus* solution suspension in normal saline. Then, these test tubes were incubated at a constant temperature of 37°C. Afterward, bacteria were pipetted from the test tubes and used to prepare consecutive dilutions by taking 0.1 mL of the original solution, then mixed with 9.9 mL of PBS. Next, 200 μL bacteria solution from the above solution was plated on solid agar and repeated 3 times for each group. After 24 h incubation, the viable number of bacteria was counted and reported as mean (CFU/mL).

In vivo Evaluation

Forty-eight male Sprague–Dawley rats (age of 4 months, body weight of 280 ± 20 g) were bought from the Animal Administration Center of Wenzhou Medical University and housed in an SPF environment with free access to food and water. Care and use of all animals conformed to the guidelines set forth by the Chinese National Institutes of Health, with relevant study protocols also approved by the Animal Care and Use Committee of Wenzhou Medical University. After 2 weeks of adaptation, two groups of rats were studied for unmodified K-wires and $(MMT/PLL\text{-}VA)_8$ multilayer films modified K-wires, respectively. All K-wires were sterilized and stored in sterile, sealed Petri dishes. The rats were intraperitoneally anesthetized with chloral hydrate. A broad area of the left knee joints was shaved, and the underlying skin washed with a povidone-iodine solution, wiped with 70% alcohol, and draped for surgery. Then, the knee joint was cut, exposing the tibial plateau. However, important nerves, blood vessels, and ligamentous tissues should be preserved as much as possible. Under sterile conditions, the medullary cavity was drilled vertically with a 0.8 mm K-bit, drilled perpendicular to the tibial plateau, and a small amount of bone marrow was aspirated with a sterile syringe. The K-wire was placed in the borehole. Then, the borehole was inoculated with 10 μL of the 10^7 cells/mL *S. aureus* suspension, which was subsequently closed with bone wax, while incisions were closed with 3–0 interrupted nylon sutures. All aseptic techniques were strictly followed throughout the operation. After the rats were anesthetized, they were kept

in isolation and provided with adequate food and water, a dry environment, and monitored daily.

The WBC and CRP levels of the rats that underwent the modeling surgeries were recorded. When killed, the wound was inspected carefully, and then performed the bacteriological examination. The metaphysis of tibial plateau was imaged and examined using small-animal X-ray fluorescence tomography (energy 45 kV, current 250 mA, integration time 200 ms, Carestream DRX) and Micro-CT system (energy 70 kVp, threshold 220, current 114μA, integration time 300 ms, Scanco Medical, Bassersdorf, Switzerland) at 4 weeks after surgeries. The tibial plateaus were fixed with 4% formalin for 72 h at 4°C. The bone volume fraction (BV/TV) and bone mineral density (BMD) of the tibial plateau were determined using built-in software.

Upon aseptic harvesting of the tibial plateau, the sample was snap-frozen with liquid nitrogen, crushed into powder form, resuspended in sterile PBS solution, and vortexed for 60 s.[43] K-wires were sonicated in sterile PBS solution for 30 min. The supernatant from the tibial plateau homogenate and K-wires were serially diluted in sterile saline, plated onto agar plate media (Thermo Fisher Scientific), and incubated at 37°C. Lastly, bacteria colonies were enumerated and normalized to bone tissue or K-wires mass.

Statistical Analysis

All data are conducted as the means ± SD. Significant differences between groups were determined using unpaired Student's *t*-test, post analysis by Tukey's honestly significant difference test and ANOVA (SPSS 18.0 software, Chicago, IL). $P < 0.05$ was considered to indicate statistical significance.

Results and Discussion

Multilayer Fabrication

Here, the fabrication of $(MMT/PLL\text{-}VA)_8$ multilayer was characterized using ellipsometry. We observed that the $(MMT/PLL\text{-}VA)_8$ multilayer films grew rapidly in a linear manner as shown in Figure 1A. The thickness of the $(MMT/PLL\text{-}VA)_2$ multilayer film was 20.7 ± 0.95 nm. In addition, after we prepared the $(MMT/PLL\text{-}VA)_4$ multilayer films, the thickness increased to 45.7 ± 1.29 nm. Eventually, our final films were about 89.7 ± 0.54 nm. These findings indicate that the polyelectrolytes were successfully deposited onto the surface. We then examined the surface morphology of the sample using SEM. Our results revealed that the surface of the $(MMT/PLL\text{-}VA)_8$ silicon wafer showed a uniform porous film structure compared with the unmodified wafer (Figure 1B and C). This proved that the surface of the silicon wafer can detect the layer of the multilayer films.

VA Release from the Multilayer Films

In this study, we design the multilayer films which can release Van when outside bacteria multiplied releasing CMS. To observe this directly, we evaluated the drug release by measuring the zone of bacterial inhibition (ZOI). During the first step, the multilayer films were immersed in 0.01 M PBS, 100 U/mL CMS, and 10^5 CFU/mL *S. aureus* for 2,

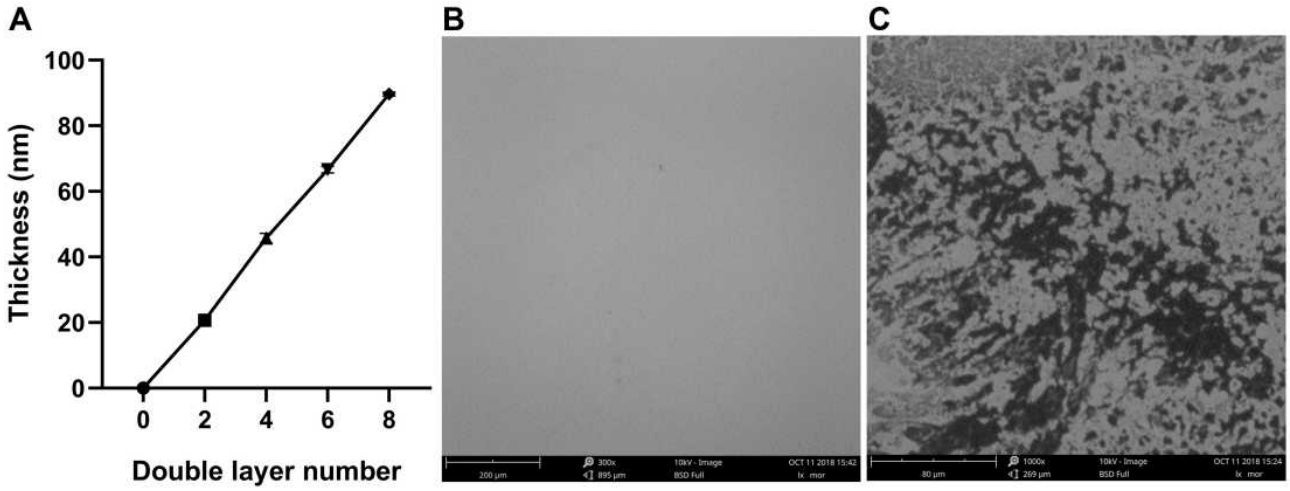

Figure 1 (**A**) Ellipsometry measurement of the $(MMT/PLL\text{-}VA)_8$ multilayer films and SEM images of (**B**) unmodified silicon wafer and (**C**) $(MMT/PLL\text{-}VA)_8$ silicon wafer.

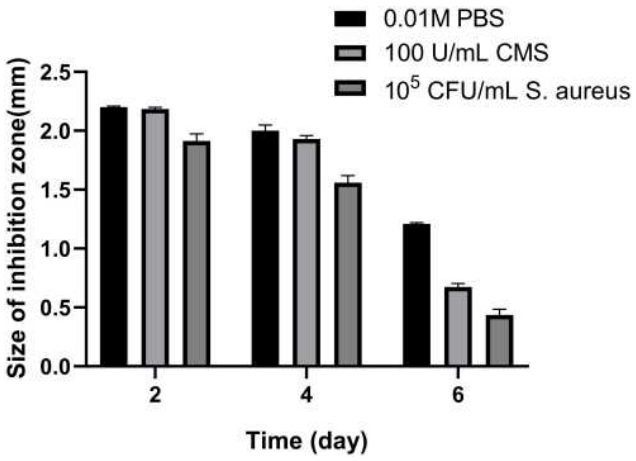

Figure 2 ZOI detection of the $(MMT/PLL\text{-}VA)_8$ multilayer films after being immersed in PBS, 100 U/mL CMS or 10^5 CFU/mL *S. aureus* on different days.

4, and 6 days. Afterward, the samples were placed on each nutrient agar media and subsequently measured the ZOI. The results are depicted in Figure 2. After immersing for 2 and 4 days, we identified that ZOI of multilayer films in PBS and CMS solutions were equal, while that of *S. aureus* solution was the smallest. After being immersed for 6 days, the ZOI of multilayer films was 1.21 ± 0.008, 0.67 ± 0.025, and 0.44 ± 0.039 mm in PBS, CMS, and *S. aureus* solutions, respectively. A reasonable explanation for this is that the CMS in the external solutions or secreted by *S. aureus* might have degraded the multilayer films, thus VA was released in solution. To ascertain this argument, we assessed the changes in thickness using spectroscopic ellipsometry (Figure 3). In general, after being immersed in PBS for 6 days, we found that the thickness of the multilayer films only changed from 85.1 ± 0.37 to 80.4 ± 0.34 nm,

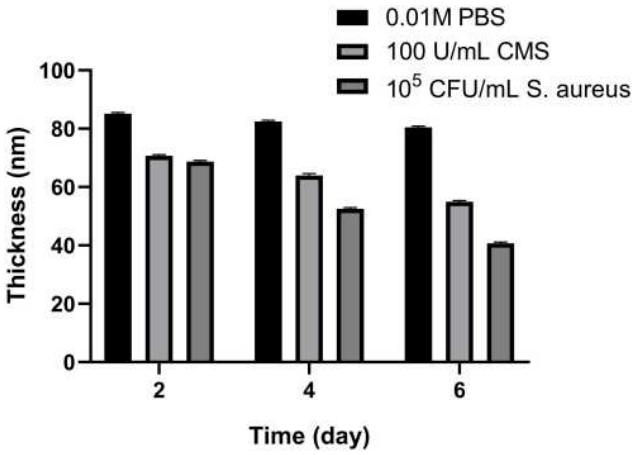

Figure 3 Ellipsometry measurement of the $(MMT/PLL\text{-}VA)_8$ multilayer films after being immersed in PBS, 100 U/mL CMS or 10^5 CFU/mL *S. aureus* on different days.

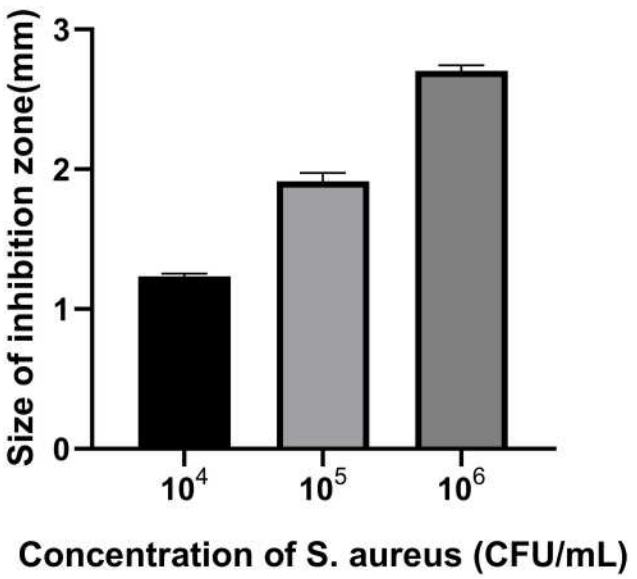

Figure 4 ZOI detection of the $(MMT/PLL\text{-}VA)_8$ multilayer films after being soaked in different concentrations of *S. aureus*.

which indicates that the multilayer films were stable. However, the thickness in *S. aureus* and CMS changed considerably. In particular, the thickness of the multilayer films after being immersed in CMS for 2, 4, and 6 days was 70.7 ± 0.36, 63.9 ± 0.54, and 54.9 ± 0.33 nm, respectively, while that of *S. aureus* after being immersed for 2, 4, and 6 days was 68.7 ± 0.37, 52.5 ± 0.37, and 40.7 ± 0.36 nm, respectively. These changes in thickness directly suggest that the multilayer film was degraded, especially in *S. aureus* and CMS solution. As a result, the measurement of ZOI corresponded with the thickness changes, hence verifying the association between the remaining VA and ZOI size.

We further measured the ZOI to evaluate the effects of bacteria and CMS concentration on the multilayer film degradation and VA release. With the increase of *S. aureus* concentration, the ZOI increased from 1.23 ± 0.017 to 2.70 ± 0.034 mm (Figure 4). This implies that as the concentration of the immersed bacteria increases, ZOI also increases. This may be attributed to the fact that after the CMS secreted from the bacteria promoted the degradation of the films, most of the film fragments remained on the surface of the substrate, but due to the degradation of the films, the drug was easier to release, thereby formed a larger bacteriostatic ring. Moreover, we studied the effect of CMS concentration on multilayer film degradation. As shown in Figure 5, when the CMS concentration was 75 U/mL, the ZOI around the films was 2.02 ± 0.048 mm. However, as the CMS concentration increased to 175 U/

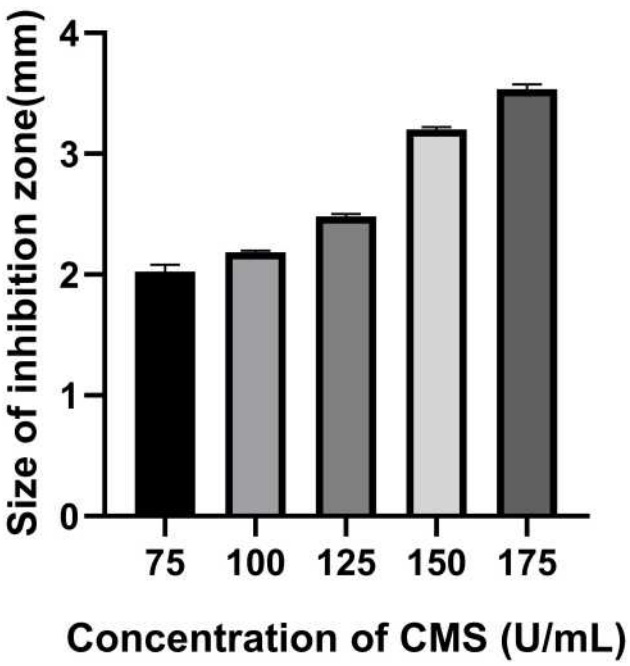

Figure 5 ZOI detection of the $(MMT/PLL\text{-}VA)_8$ multilayer films after being soaked in different concentrations of CMS.

mL, the ZOI also increased to 3.53 ± 0.034 mm. Remarkably, this result was consistent with the finding in Figure 3, whereby increasing CMS concentration accelerated the multilayer film degradation and VA release. Nevertheless, when the CMS concentration became higher than 150 U/mL, the ZOI did not change.

Effect of Multilayer Films on Cell Proliferation of Osteoblasts

Using MTT assay, it was reassuring that multilayer films depicted great cell viability against osteoblasts (Figure 6). After culturing for 1, 3, 5, and 7 days in vitro, we noted that with the increase in breeding time, the absorbance of the three groups increased accordingly. We also observed that multilayer films exhibited no obvious cytotoxicity; thus, the cells could spread on the surface of the multilayer films.

In vitro Antibacterial Tests

The results of the antibacterial assay were robustly confirmed using SEM analysis (Figure 7). Herein, numerous distinguishable *S. aureus* cells were found distributed on unmodified silicon wafers after 8 h of incubation. On the other hand, SEM also showed no bacteria on the surface of $(MMT/PLL\text{-}VA)_8$ multilayer films silicon wafers, indicating the death of *S. aureus*. To deeply understand the antibacterial effect of $(MMT/PLL\text{-}VA)_8$ multilayer film more accurately,

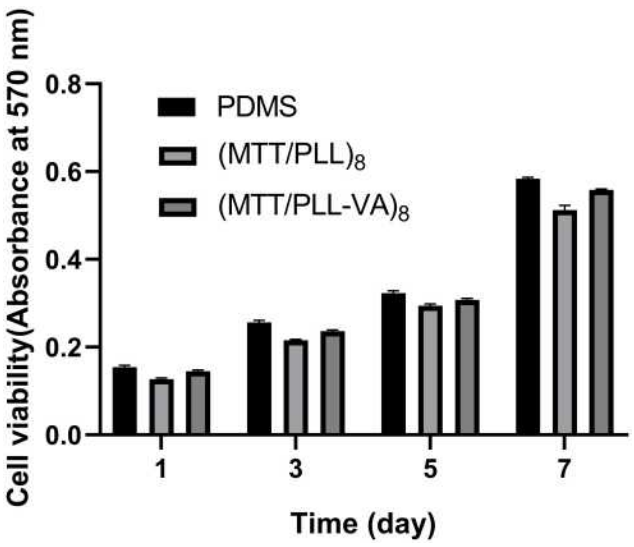

Figure 6 MTT assay for cellular viability.

we subsequently performed inhibition rate assays. We used *S. aureus* to evaluate the bactericidal capabilities of the $(MMT/PLL\text{-}VA)_8$ multilayer films because it is one of the most prevalent pathogens, found in endosseous implant infection. In this study, the *S. aureus* strains and solutions were plated on an agar plate to determine viable counts. As presented in Figure 8, we observed that the number of bacteria in contact with unmodified PDMS increased significantly in the first 2 h and then progressively decreased in the following 24 h. However, after the samples were incubated with *S. aureus* solutions, the bacteria in $(MMT/PLL\text{-}VA)_8$ group rapidly decreased in the first 4 h and then died at 24 h. This perhaps might be due to CMS released when outside bacteria multiplied, resulting in the degradation of the multilayer films, thereby releasing VA from the system killing bacteria rapidly.

In vivo Evaluation

During the post-implantation investigation, blood samples of rats were retrieved for analysis of WBC and CRP of rats at predetermined time intervals (Figure 9). These infection parameters proved a distinguishing difference between the two groups. After 7 days of implantation, the unmodified group exhibited high WBC and CRP levels due to foreign body reactions and lack of antibiotics. Subsequently, the WBC and CRP indicators of rats for the unmodified group remained higher compared with the $(MMT/PLL\text{-}VA)_8$ group. Additionally, the WBC and CRP levels in the $(MMT/PLL\text{-}VA)_8$ group declined over time and then returned to a normal level after 28 days. Herein, we

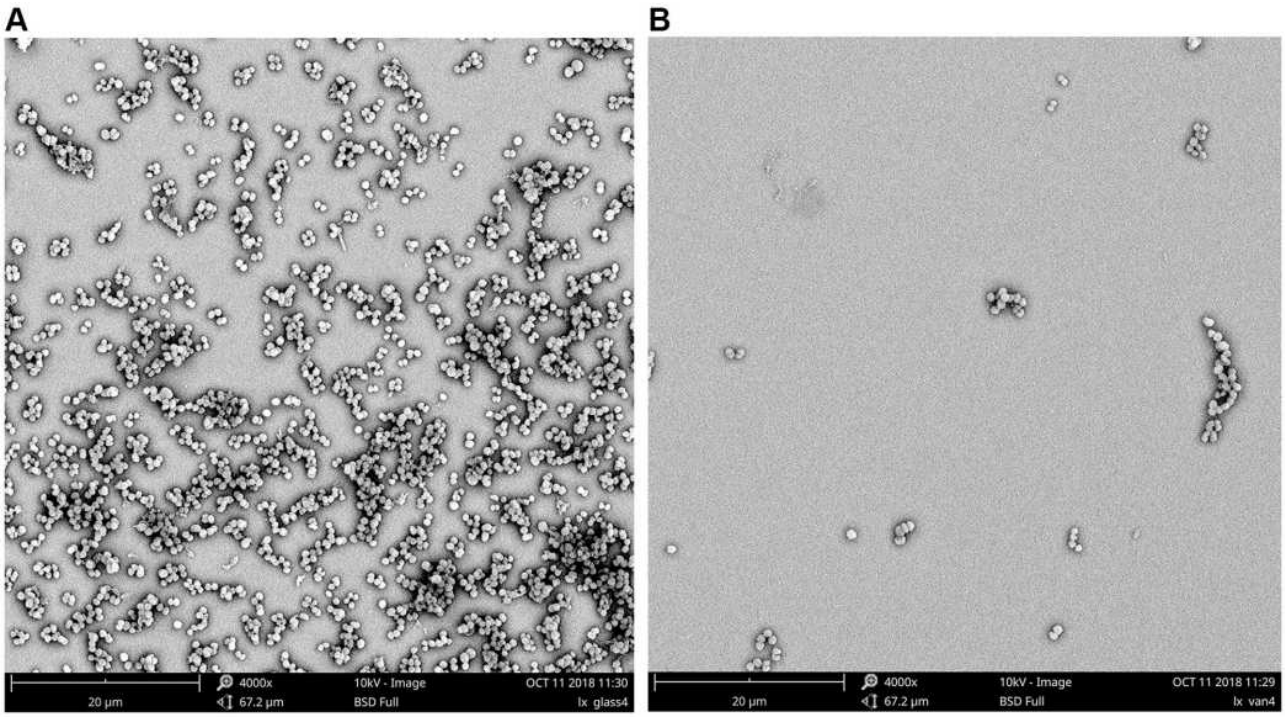

Figure 7 Scanning electron microscopy (SEM) analysis of *S. aureus* adhesions on (**A**) unmodified and (**B**) $(MMT/PLL\text{-}VA)_8$ multilayer films silicon wafers.

noted that without antibacterial drugs, it was not effective to control infection satisfactorily. More interestingly, after incubation on agar plates, we isolated a considerable amount of bacterial pathogens in the unmodified group, but no bacteria were detected in the $(MMT/PLL\text{-}VA)_8$ group (Figure 10). Taken together, the comparison between the two groups revealed the very efficient treatment of the $(MMT/PLL\text{-}VA)_8$ group infections.

In addition, our results, based on the X-ray analysis, demonstrated that the lateral tibial plateau of the unmodified group was characterized by an irregular partially

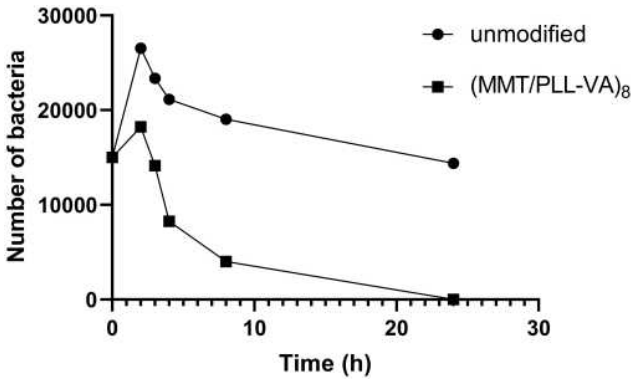

Figure 8 Changes in the viable *S. aureus* cells with the time of exposure to pristine unmodified or $(MMT/PLL\text{-}VA)_8$ multilayer films.

osteolytic lesion (Figure 11A). On the other hand, the $(MMT/PLL\text{-}VA)_8$ group showed normal bone morphology with no lesions (Figure 11B).

We further used Micro-CT to perform imaging evaluation of bone specimens obtained after 4 weeks of implantation and made 3-D reconstructions based on built-in software. Our findings elucidated that rats in the unmodified group exhibited the slowest rate of bone bridging and regeneration. The yellow part of the figure represents the new bone, whereby only a small amount of new bone was formed after 4 weeks (Figure 11C). More importantly, we uncovered that $(MMT/PLL\text{-}VA)_8$ group performed well (Figure 11D). In order to get a more accurate conclusion, we further conducted a quantitative analysis. The evaluation was performed using a micro CT on bone specimens obtained 4 weeks after implantation. It has been shown that micro CT can provide values for mineralized bone tissue which can be supported by histology. The bone mineral density (BMD) and bone volume fraction (BV/TV) of the tibial plateau were tested for quantitative analysis. We subsequently identified that bone volume fraction in the unmodified group markedly decreased compared with that of the $(MMT/PLL\text{-}VA)_8$ group (Figure 12A). Similarly, we observed that

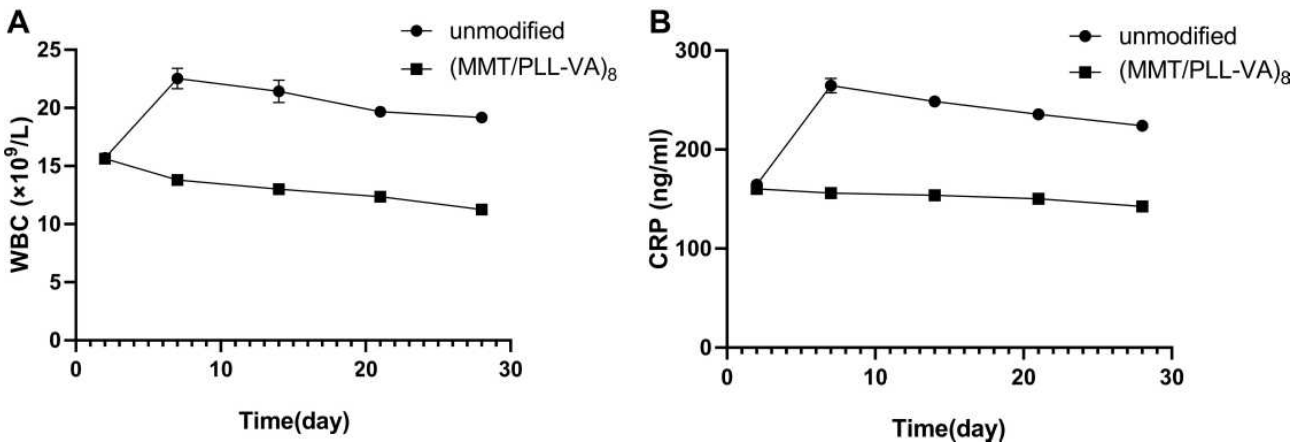

Figure 9 (**A**) Changes in WBC count. (**B**) Changes in CRP levels of rats implanted with different K-wires.

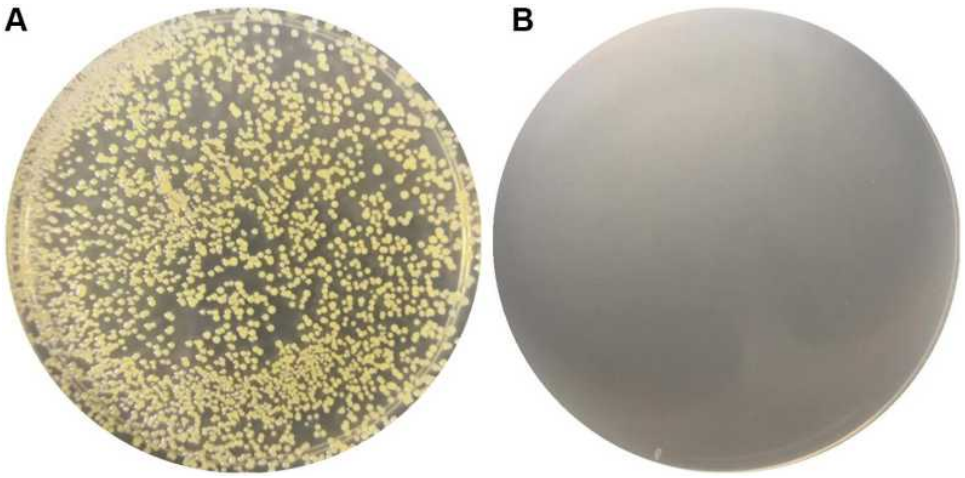

Figure 10 Swabs for bacteriological examination were taken from all wounds of (**A**) unmodified group and (**B**) $(MMT/PLL\text{-}VA)_8$ group after the rats were euthanised.

BMD of the tibial plateau of the rats in the unmodified group was significantly decreased than that of the $(MMT/PLL\text{-}VA)_8$ group (Figure 12B). These findings could be explained by the "race to the surface theory" in which bone regeneration required a high level of sterility while bacteria would seriously obstruct the bone regeneration process.[44,45] Of noteworthy, groups implanted with $(MMT/PLL\text{-}VA)_8$ showed great bone binding in the fracture sites due to their ability to release VA from the multilayer films for the great treatment of the bone infection and enhanced bone repair. Compared with the unmodified group, there was an average 5.73 and 7.17 log reductions of *S. aureus* in the bone and on the surface of K-wire in the $(MMT/PLL\text{-}VA)_8$ group, respectively (Figure 13A and B).

Conclusion

In summary, this present research shows that $(MMT/PLL\text{-}VA)_8$ multilayer films obtained via layer-by-layer (LbL) assembly exhibited linear growth. Notably, multilayer films were progressively degraded and showed well concentration-dependent degradation characteristics following incubation with CMS or bacterium solution. Additionally, VA depicted on-demand property which was triggered intelligently by CMS or bacterium solution, while the MTT analysis proved that the multilayer film was characterized by good biocompatibility. The

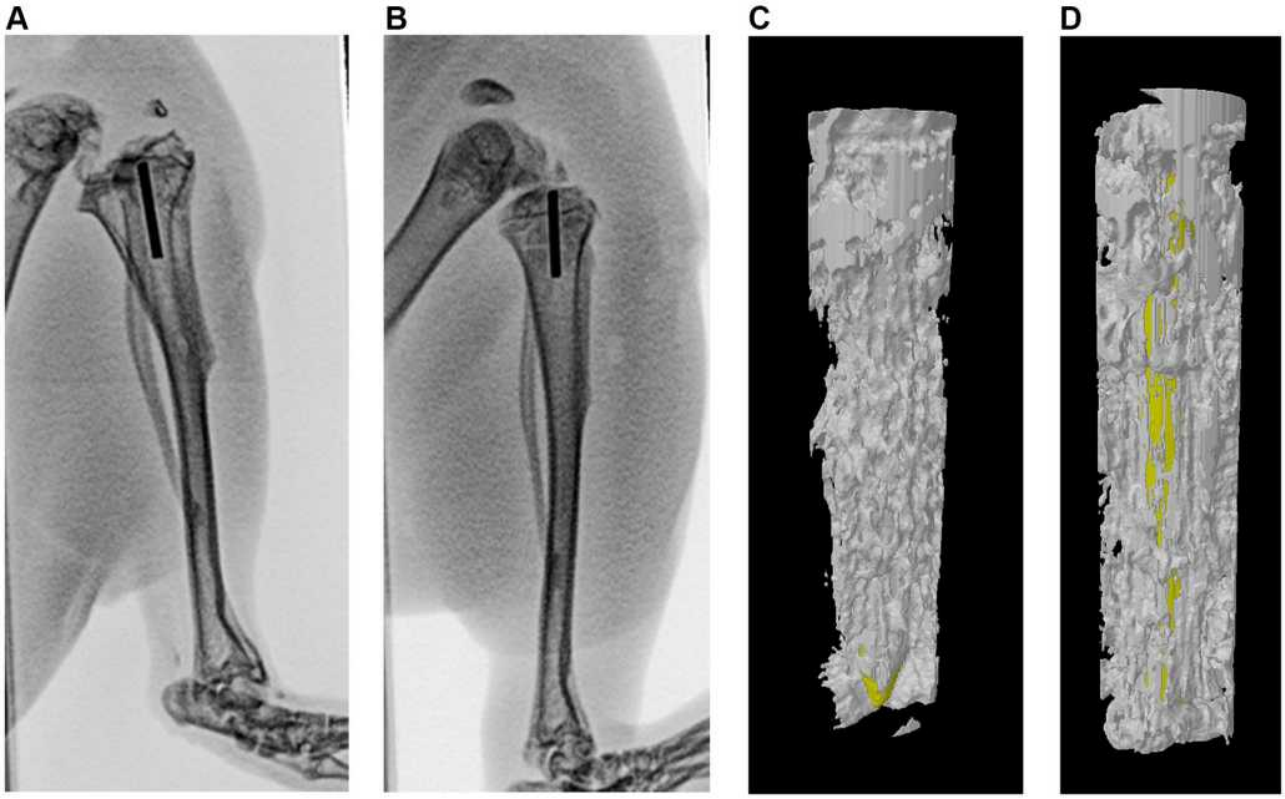

Figure 11 X-ray results after 4 weeks of modeling, (**A** and **B**) unmodified group, $(MMT/PLL\text{-}VA)_8$ group. 4 weeks after implantation, micro-CT images of the bone specimens. New bone formation around the Kirschner wires, (**C** and **D**) unmodified group, $(MMT/PLL\text{-}VA)_8$ group.

results of in vitro bacterial shake-flask method showed high levels of bactericidal activity, whereas in the in vivo antibacterial tests, the K-wires coated with $(MMT/PLL\text{-}VA)_8$ multilayer films exhibited lower infections incidence and inflammation than the unmodified K-wires. Further, in vivo studies demonstrate the

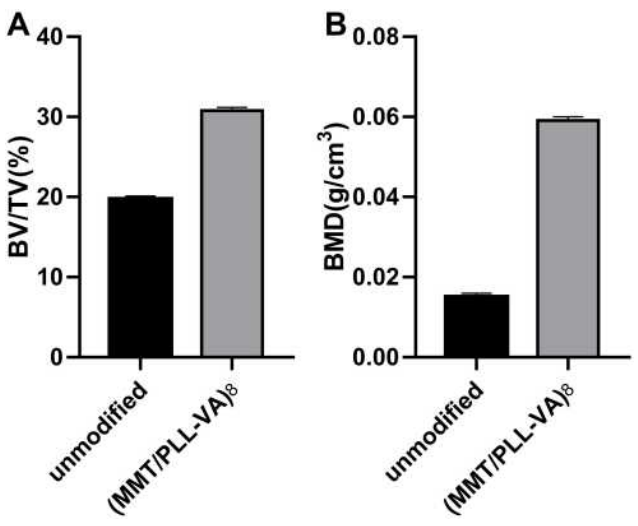

Figure 12 Quantitative analysis of bone mineral density (BMD) (**A**) and bone volume fraction (BV/TV) (**B**) after surgery.

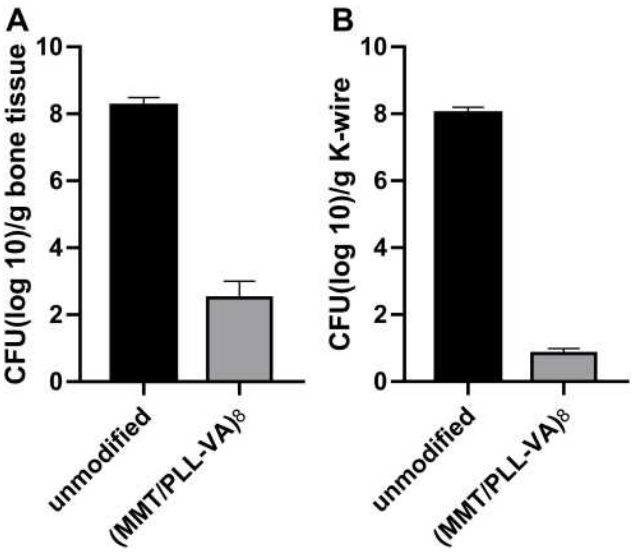

Figure 13 Bacteria recovered from (**A**) bone tissue and (**B**) implanted K-wire.

potential to provide more evidence for the use of this biomaterial to mitigate bone infection.

Acknowledgments

We are grateful to the participants involved in this study.

Disclosure

The authors reported no conflicts of interest for this work.

References

1. Bottagisio M, Coman C, Lovati AB. Animal models of orthopaedic infections. A review of rabbit models used to induce long bone bacterial infections. *J Med Microbiol*. 2019;68(4):506–537. doi:10.1099/jmm.0.000952
2. Rupp M, Popp D, Alt V. Prevention of infection in open fractures: where are the pendulums now? *Injury*. 2019.
3. Høiby N, Bjarnsholt T, Givskov M, Molin S, Ciofu O. Antibiotic resistance of bacterial biofilms. *Int J Antimicrob Agents*. 2010;35 (4):322–332. doi:10.1016/j.ijantimicag.2009.12.011
4. Veerachamy S, Yarlagadda T, Manivasagam G, Yarlagadda PK. Bacterial adherence and biofilm formation on medical implants: a review. *Proc Inst Mech Eng H*. 2014;228(10):1083–1099. doi:10.1177/0954411914556137
5. Hall CW, Mah TF. Molecular mechanisms of biofilm-based antibiotic resistance and tolerance in pathogenic bacteria. *FEMS Microbiol Rev*. 2017;41(3):276–301. doi:10.1093/femsre/fux010
6. Bue M, Hanberg P, Koch J, et al. Single-dose bone pharmacokinetics of vancomycin in a porcine implant-associated osteomyelitis model. *J Orthop Res*. 2018;36(4):1093–1098. doi:10.1002/jor.23776
7. Darouiche RO. Treatment of infections associated with surgical implants. *N Engl J Med*. 2004;350(14):1422–1429. doi:10.1056/NEJMra035415
8. Flock JI, Brennan F. Antibodies that block adherence of to fibronectin. *Trends Microbiol*. 1999;7(4):140–141. doi:10.1016/S0966-842X(99)01483-3
9. Ketonis C, Dwyer J, Ilyas AM. Timing of debridement and infection rates in open fractures of the hand: a systematic Review. *Hand (N Y)*. 2017;12(2):119–126. doi:10.1177/1558944716643294
10. Hebert JS, Rehani M, Stiegelmar R. Osseointegration for lower-limb amputation: a systematic review of clinical outcomes. *JBJS Rev*. 2017;5(10):e10. doi:10.2106/JBJS.RVW.17.00037
11. Lora-Tamayo J, Senneville É, Ribera A, et al. The not-so-good prognosis of streptococcal periprosthetic joint infection managed by implant retention: the results of a large Multicenter Study. *Clin Infect Dis*. 2017;64(12):1742–1752. doi:10.1093/cid/cix227
12. He M, Wang Q, Zhao W, Zhao C. A substrate-independent ultrathin hydrogel film as an antifouling and antibacterial layer for a microfiltration membrane anchored via a layer-by-layer thiol-ene click reaction. *J Mater Chem B*. 2018;6(23):3904–3913. doi:10.1039/C8TB00937F
13. Lv H, Chen Z, Yang X, Cen L, Zhang X, Gao P. Layer-by-layer self-assembly of minocycline-loaded chitosan/alginate multilayer on titanium substrates to inhibit biofilm formation. *J Dent*. 2014;42 (11):1464–1472. doi:10.1016/j.jdent.2014.06.003
14. Huang TW, Lu HT, Ho YC, Lu KY, Wang P, Mi FL. A smart and active film with tunable drug release and color change abilities for detection and inhibition of bacterial growth. *Mater Sci Eng C*. 2021;118:111396. doi:10.1016/j.msec.2020.111396
15. Chambre L, Rosselle L, Barras A, et al. Photothermally active cryogel devices for effective release of antimicrobial peptides: on-demand treatment of infections. *ACS Appl Bio Mater*. 2020;12 (51):56805–56814. doi:10.1021/acsami.0c17633
16. Hu J, Quan Y, Lai Y, et al. A smart aminoglycoside hydrogel with tunable gel degradation, on-demand drug release, and high antibacterial activity. *J Control Release*. 2017;247:145–152. doi:10.1016/j.jconrel.2017.01.003
17. Huang J, Ren J, Chen G, et al. Tunable sequential drug delivery system based on chitosan/hyaluronic acid hydrogels and PLGA microspheres for management of non-healing infected wounds. *Mater Sci Eng C*. 2018;89:213–222. doi:10.1016/j.msec.2018.04.009
18. Nolt B, Tu F, Wang X, et al. Lactate and Immunosuppression in Sepsis. *Shock*. 2018;49(2):120–125. doi:10.1097/SHK.0000000000000958
19. Vornhagen J, Adams Waldorf KM, Rajagopal L. Perinatal group B streptococcal infections: virulence factors, immunity, and prevention strategies. *Trends Microbiol*. 2017;25(11):919–931. doi:10.1016/j.tim.2017.05.013
20. Ramsay JD, Evanoff R, Mealey RH, Simpson EL. The prevalence of elevated gamma-glutamyltransferase and sorbitol dehydrogenase activity in racing Thoroughbreds and their associations with viral infection. *Equine Vet J*. 2019;51(6):738–742. doi:10.1111/evj.13092
21. Matsusaki M, Ajiro H, Kida T, Serizawa T, Akashi M. Layer-by-layer assembly through weak interactions and their biomedical applications. *Adv Mater*. 2012;24(4):454–474. doi:10.1002/adma.201103698
22. Monge C, Almodóvar J, Boudou T, Picart C. Spatio-temporal control of LbL films for biomedical applications: from 2D to 3D. *Adv Healthcare Mater*. 2015;4(6):811–830. doi:10.1002/adhm.201400715
23. Vander Straeten A, Bratek-Skicki A, Jonas AM, Fustin CA, Dupont-Gillain C. Integrating proteins in layer-by-layer assemblies independently of their electrical charge. *ACS Nano*. 2018;12(8):8372–8381. doi:10.1021/acsnano.8b03710
24. Zhou B, Hu X, Zhu J, Wang Z, Wang X, Wang M. Release properties of tannic acid from hydrogen bond driven antioxidative cellulose nanofibrous films. *Int J Biol Macromol*. 2016;91:68–74. doi:10.1016/j.ijbiomac.2016.05.084
25. Kim BS, Park SW, Hammond PT. Hydrogen-bonding layer-by-layer-assembled biodegradable polymeric micelles as drug delivery vehicles from surfaces. *ACS Nano*. 2008;2(2):386–392. doi:10.1021/nn700408z
26. Tian Y, He Q, Tao C, Cui Y, Ai S, Li J. Fabrication of polyethyleneimine and poly(styrene-alt-maleic anhydride) nanotubes through covalent bond. *J Nanosci Nanotechnol*. 2006;6(7):2072–2076. doi:10.1166/jnn.2006.369
27. Correa S, Dreaden EC, Gu L, Hammond PT. Engineering nanolayered particles for modular drug delivery. *J Control Release*. 2016;240:364–386. doi:10.1016/j.jconrel.2016.01.040
28. BinAhmed S, Hasane A, Wang Z, Mansurov A, Romero-Vargas Castrillón S. Bacterial adhesion to ultrafiltration membranes: role of hydrophilicity, natural organic matter, and cell-surface macromolecules. *Environ Sci Technol*. 2018;52(1):162–172. doi:10.1021/acs.est.7b03682
29. Musil J. Flexible antibacterial coatings. *Molecules*. 2017;22(5):813. doi:10.3390/molecules22050813
30. Stewart S, Barr S, Engiles J, et al. Vancomycin-modified implant surface inhibits biofilm formation and supports bone-healing in an infected osteotomy model in sheep: a proof-of-concept study. *J Bone Joint Surg*. 2012;94(15):1406–1415. doi:10.2106/JBJS.K.00886
31. Mochalin VN, Pentecost A, Li XM, et al. Adsorption of drugs on nanodiamond: toward development of a drug delivery platform. *Mol Pharm*. 2013;10(10):3728–3735. doi:10.1021/mp400213z
32. Popat KC, Eltgroth M, Latempa TJ, Grimes CA, Desai TA. Decreased Staphylococcus epidermis adhesion and increased osteoblast functionality on antibiotic-loaded titania nanotubes. *Biomaterials*. 2007;28 (32):4880–4888. doi:10.1016/j.biomaterials.2007.07.037
33. Bhandari V, Wong KS, Zhou JL, Mabanglo MF, Batey RA, Houry WA. The role of clpp protease in bacterial pathogenesis and human diseases. *ACS Chem Biol*. 2018;13(6):1413–1425. doi:10.1021/acschembio.8b00124
34. Szafranski SP, Winkel A, Stiesch M. The use of bacteriophages to biocontrol oral biofilms. *J Biotechnol*. 2017;250:29–44. doi:10.1016/j.jbiotec.2017.01.002

35. Arciola CR, Campoccia D, Montanaro L. Implant infections: adhesion, biofilm formation and immune evasion. *Nat Rev Microbiol*. 2018;16(7):397–409. doi:10.1038/s41579-018-0019-y
36. Ma L, Hu P, Wu ZQ, Song XZ. Clinical application of vacuum sealing drainage combined with chymotrypsin in the treatment of post-traumatic mandibular osteomyelitis. *Chin J Stomatology*. 2018;53(2):123–124.
37. Rivers JK, Mistry BD. Soft-tissue infection caused by streptococcus anginosus after intramucosal hyaluronidase injection: a rare complication related to dermal filler injection. *Dermatol Surg*. 2018;44 (Suppl 1):S51–s53. doi:10.1097/DSS.0000000000001625
38. Zhang Y, Shen L, Wang P, et al. Treatment with vancomycin loaded calcium sulphate and autogenous bone in an improved rabbit model of bone infection. *J Vis Exp*. 2019;145.
39. Wei P, Jing W, Yuan Z, et al. Vancomycin- and strontium-loaded microspheres with multifunctional activities against bacteria, in angiogenesis, and in osteogenesis for enhancing infected bone regeneration. *ACS Appl Mater Interfaces*. 2019;11 (34):30596–30609. doi:10.1021/acsami.9b10219
40. Bariteau JT, Kadakia RJ, Traub BC, Viggeswarapu M, Willett NJ. Impact of vancomycin treatment on human mesenchymal stromal cells during osteogenic differentiation. *Foot Ankle Int*. 2018;39 (8):954–959. doi:10.1177/1071100718766655
41. Xu Q, Li X, Jin Y, et al. Bacterial self-defense antibiotics release from organic-inorganic hybrid multilayer films for long-term anti-adhesion and biofilm inhibition properties. *Nanoscale*. 2017;9 (48):19245–19254. doi:10.1039/C7NR07106J
42. Zelzer M, Todd SJ, Hirst AR, McDonald TO, Ulijn RV. Enzyme responsive materials: design strategies and future developments. *Biomater Sci*. 2013;1(1):11–39. doi:10.1039/C2BM00041E
43. Shiels SM, Bouchard M, Wang H, Wenke JC. Chlorhexidine-releasing implant coating on intramedullary nail reduces infection in a rat model. *Eur Cell Mater*. 2018;35:178–194. doi:10.22203/eCM.v035a13
44. Trobos M, Juhlin A, Shah F, Hoffman M, Sahlin H, Dahlin C. In vitro evaluation of barrier function against oral bacteria of dense and expanded polytetrafluoroethylene (PTFE) membranes for guided bone regeneration. *Clin Implant Dent Relat Res*. 2018;20 (5):738–748. doi:10.1111/cid.12629
45. Yu Y, Jin G, Xue Y, Wang D, Liu X, Sun J. Multifunctions of dual Zn/Mg ion co-implanted titanium on osteogenesis, angiogenesis and bacteria inhibition for dental implants. *Acta Biomater*. 2017;49:590–603. doi:10.1016/j.actbio.2016.11.067